

Fluctuational Instabilities of Alkali and Noble Metal Nanowires

J. Bürki, C.A. Stafford, and D.L. Stein

Department of Physics, University of Arizona, 1118 E. 4th St., Tucson, AZ, USA

ABSTRACT

We introduce a continuum approach to studying the lifetimes of monovalent metal nanowires. By modelling the thermal fluctuations of cylindrical nanowires through the use of stochastic Ginzburg-Landau classical field theories, we construct a self-consistent approach to the fluctuation-induced “necking” of nanowires. Our theory provides quantitative estimates of the lifetimes for alkali metal nanowires in the conductance range $10 < G/G_0 < 100$ (where $G_0 = 2e^2/h$ is the conductance quantum), and allows us to account for qualitative differences in the conductance histograms of alkali vs. noble metal nanowires.

Keywords: Nanowires, Lifetime, Thermal fluctuations

1. INTRODUCTION

A metallic nanowire, defined as a wire whose thinnest cross-section contains only a few, to a few hundred, atoms, acts essentially as an incompressible fluid of electrons, at least for simple monovalent metals, such as the alkali or noble metals. One would therefore expect a long cylindrical nanowire to break apart due to the Rayleigh instability. Long gold nanowires have nevertheless been observed in transmission electron microscopy (TEM) experiments,^{1,2} and in fact appear to be surprisingly stable, with lifetimes of the order of seconds. This apparent paradox has been resolved theoretically³⁻⁵ with the inclusion of quantum-size effects, which have been shown to stabilize the wires for a set of “magic” radii. The stability thus arises through a competition of shell-effects, comparable to what happens in metal clusters, and an interplay of Rayleigh and Peierls instabilities. Linear stability analyses have shown cylindrical nanowires to be very stable, while a dynamical model, including surface self-diffusion, indicates that they should form spontaneously from random initial wires.⁶

Despite their robustness, cylindrical wires are nevertheless only metastable, with finite lifetimes in the presence of thermal fluctuations. In this paper, we introduce a continuum approach to studying the lifetimes of monovalent metal nanowires. The ionic medium is treated as an incompressible continuum (jellium), and electron-shell effects are treated semiclassically. This approach appears very promising for studying nanowires of “intermediate” thickness, which are thin enough that electron-shell effects play a dominant role, but not so thin that a continuum approach is unjustified. Thermal fluctuations are modelled through the use of stochastic Ginzburg-Landau classical field theories, and we construct a self-consistent approach to the fluctuation-induced “necking” of nanowires. Our theory provides quantitative estimates of the lifetimes for alkali nanowires with electrical conductance G in the range $10 < G/G_0 < 100$, where $G_0 = 2e^2/h$ is the conductance quantum. Moreover, our theory accounts qualitatively for the large difference in the observed stability of alkali vs. noble metal nanowires.

The paper is organized as follows: In section 2, we give a brief survey of the phenomenology of nanowires, with particular emphasis on the results that are relevant to the lifetime of nanowires. The continuum free-electron model is presented in section 3, while sections 4-7 describe the field theory from which the lifetime is computed. Finally, section 8 is devoted to discussion and analysis of the results, with comparison to existing experiments.

2. PHENOMENOLOGY OF NANOWIRES

Metallic nanowires have been extensively studied in the past decade.⁷⁻¹⁴ Originally, short thin contacts were formed by crashing the gold tip of a scanning tunneling microscope (STM) into a gold sample. Upon subsequent retraction of the tip, the contact gradually necked down until it broke, and the electrical conductance through the contact was recorded. An atomic force microscope was used to simultaneously measure the tensile force applied to the contact. Conductance plateaus at integer multiples of G_0 were observed, together with a sawtooth behavior

of the force, with a perfect correlation between abrupt changes in both quantities. Because of the inherent irreproducibility of the measurements – wires have a different structure on each cycle – and the imperfection of the conductance quantization, statistical analyses have turned out to be very useful. A different setup, the mechanically controllable break junction (MCBJ),¹⁵ has been used in most statistical studies. In this technique, a notched wire is glued to a substrate, whose bending is used to deform the contact. By breaking the wire and putting it back together, one can form a nanocontact, which can be repeatedly broken and reformed. Conductance histograms,^{10–13} built out of thousands of conductance traces, have clear peaks at positions close to, but below, integer multiples of the conductance quantum G_0 . Which peaks are present depends on the metal considered: For example, gold has all peaks $1, 2, 3, 4, \dots G_0$,^{10, 12} while sodium has large peaks at $G = 1, 3, 5, 6, \dots G_0$,¹¹ with only smaller peaks at $G = 2, 4 \dots G_0$.¹⁶ The shift and broadening of the peaks have been shown to be due to disorder^{17–19} both in the contact and the leads, either in the form of impurities, or more likely, of surface corrugation due to the imperfect atomic structure.

More recently, the MCBJ technique has been used to build histograms for alkali metal nanocontacts with larger conductances.^{20–22} Peaks have been found to persist up to conductances $\simeq 100G_0$, while the peak positions are periodic in \sqrt{G} . This is evidence for shell-filling effects, comparable to what happens in metal clusters. The amplitude of the peaks has been found to be further periodically modulated, reflecting a supershell structure.²¹ The same type of shell effects have recently been observed for gold nanowires.^{23, 24} These experiments, though not directly accessing the lifetime of nanowires, still provide some information about it: A nanowire might be stable to small perturbations, but not give rise to a peak in a conductance histogram provided its lifetime is short compared to the rate of deformation of the contact in the experiment. The observation of a given peak therefore gives access to a lower bound of the lifetime of the corresponding wire.

Imaging experiments^{1, 2, 25–28} using TEM give a more direct access to the lifetime of nanowires, and produce long cylindrical wires which are more easily treated theoretically. Holes are burned through a thin gold film using an intense electron beam, leaving a suspended nanowire when two holes come close together. Such a wire is often found to evolve into a long, nearly perfect cylindrical wire, which connects to macroscopic contacts at two well-defined junctions.¹ Under electron-beam irradiation, the wires are observed to thin via the nucleation of a surface kink at one end, and the subsequent propagation of the kink along the wire until it is absorbed in the other contact. Although no systematic study of the lifetime of such wires is available, they have been reported to remain stable for seconds^{1, 2} despite the strong electron irradiation necessary for the imaging process.

3. THE MODEL

We use a nanoscale free-electron model²⁹ in which the atomic structure of the wire is replaced by a continuous positive background of constant charge density. We restrict ourselves to wires with axial symmetry (which includes the most stable wires³⁰), described by the radius of the wire $R(z, t)$ at time t and position z along the wire axis. Free and independent electrons are confined within the wire by hard-walls. The nanowire is in electrical contact with macroscopic metallic electrodes,^{1, 2} so the relevant thermodynamic potential for the electrons is the grand-canonical potential

$$\Omega_e(T, \mu_e) = -k_B T \int dE g(E) \ln \left(1 + e^{-\frac{E - \mu_e}{k_B T}} \right) \quad (1)$$

at temperature T and electrochemical potential μ_e , k_B being the Boltzmann constant (which will hereafter be set to one). An expansion of Ω in terms of geometrical quantities can generically be written^{31, 32} as

$$\Omega_e = -\omega \mathcal{V} + \sigma \mathcal{S} - \gamma \mathcal{C} + \delta\Omega, \quad (2)$$

where $\mathcal{V}, \mathcal{S}, \mathcal{C}$ are respectively the volume, surface area and integrated mean curvature of the wire, and ω, σ, γ are material and temperature dependent coefficients. $\delta\Omega$ is a fluctuating term giving quantum corrections to the otherwise smooth expansion of Ω .

Assuming the radius of the wire changes slowly compared to the Fermi wavelength λ_F , the fluctuating term $\delta\Omega$ can be written as

$$\delta\Omega = \int dz V_{shell}(R(z), T), \quad (3)$$

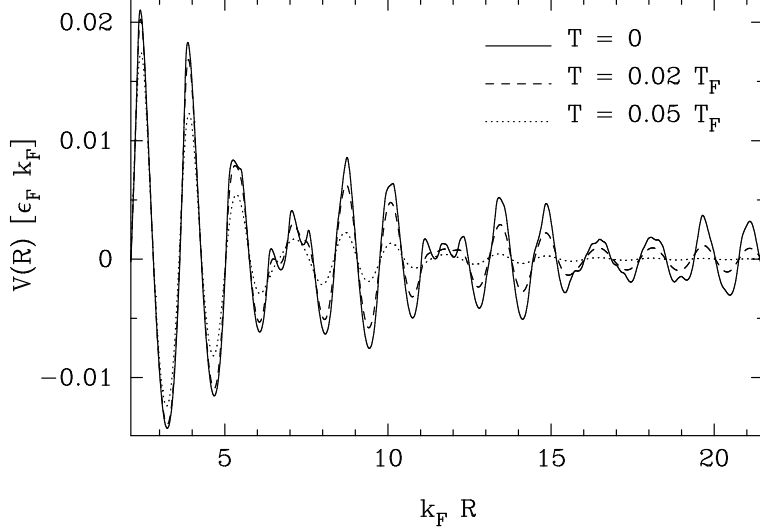


Figure 1. Electron-shell potential $V_{shell}(R, T)$ at zero and two finite temperatures, which correspond respectively to 1000K and 2500K for Na. The electrical conductance values of the principal wires studied in this article are indicated on the upper horizontal axis.

where $V_{shell}(R, T)$ is the electron-shell potential, shown in Fig. 1 for three different temperatures. This potential is responsible for the stability of metallic nanowires, its minima corresponding to the “magic” radii mentioned above, and can be computed in the semiclassical approximation using a Gutzwiller-type trace formula as⁶

$$V_{shell}(R, T) = \frac{2\varepsilon_F}{\pi} \sum_{w=1}^{\infty} \sum_{v=2w}^{\infty} a_{vw}(T) \frac{f_{vw} \cos \theta_{vw}}{v^2 L_{vw}}, \quad (4)$$

where the sum includes all classical periodic orbits (v, w) in a disk billiard,³¹ characterized by their number of vertices v and winding number w , $L_{vw} = 2vR \sin(\pi w/v)$ is the length of orbit (v, w) , and $\theta_{vw} = k_F L_{vw} - 3v\pi/2$. The factor $f_{vw} = 1$ for $v = 2w$, $f_{vw} = 2$ otherwise, accounts for the invariance under time-reversal symmetry of some orbits, and $a_{vw}(T) = \tau_{vw} / \sinh \tau_{vw}$ ($\tau_{vw} = \pi k_F L_{vw} T / 2T_F$) is a temperature-dependent damping factor.

Such a model has been successful in explaining many of the observed phenomena in monovalent metallic nanowires: sawtooth behavior of the tensile force, correlated with conductance steps²⁹; conductance histograms¹⁸; spontaneous formation⁶ and stability³⁻⁵ of long cylindrical nanowires; shell and super-shell structure in conductance histograms,³⁰ etc. The latter study relaxed the restriction to axial symmetry, showing that the most stable wires are indeed cylindrical, with a few exceptions at low conductance, where a few additional stable wires with elliptic cross-sections have been found. One may conclude that deformations breaking the axial symmetry can essentially be ignored for thicker wires, due to their large surface energy cost.

In the spirit of the Born-Oppenheimer approximation, the electronic energy functional (2) is taken as the potential energy of the ionic medium. The nanowire is in contact with metallic electrodes, with which it can exchange atoms via surface self-diffusion.⁶ The relevant thermodynamic potential for the atoms is thus

$$\Omega_a = \Omega_e - \mu_a \mathcal{V} / \mathcal{V}_a, \quad (5)$$

where μ_a is the chemical potential for a surface atom in the contacts, and $\mathcal{V}_a = 3\pi^2/k_F^3$ is the volume of an atom. Eq. (5) is a functional of the geometry of the contact, and is the basis for our field-theory. The term proportional to the mean curvature in Eq. (2) has a contribution from the transverse curvature, which is proportional to the length L of the wire, and a contribution from the longitudinal curvature, which is only a few percent of the surface energy, and can therefore be neglected. As a result, the energy (5) becomes

$$\Omega_a = \int dz \left[2\pi\sigma R(z, t) \sqrt{1 + (\partial_z R)^2} - \pi\gamma + V_{shell}(R, T) \right] - (\omega + \mu_a / \mathcal{V}_a) \mathcal{V}, \quad (6)$$

where $\partial_z R$ is the derivative of $R(z, t)$ with respect to z .

We are considering the lifetime of perfect cylinders of length L , so that the radius function may be written as a constant plus fluctuations,

$$R(z, t) \equiv R_0 + \phi(z, t). \quad (7)$$

A stable cylindrical nanowire of radius R_0 represents a state of diffusive equilibrium between the wire and the contacts, for which

$$\frac{\mu_a}{\mathcal{V}_a} = \frac{1}{2\pi R_0} \frac{\partial}{\partial R_0} \left(\frac{\Omega_e(R_0)}{L} \right) = \frac{\sigma}{R_0} - \omega + \frac{1}{2\pi R_0} \frac{\partial V_{shell}(R_0)}{\partial R_0}, \quad (8)$$

where $\Omega_e(R_0)$ is the electronic energy of an unperturbed cylinder. The most stable nanowires correspond to minima of $V_{shell}(R_0)$ (c.f. Fig. 1), for which Eq. (8) simplifies to

$$\frac{\mu_a}{\mathcal{V}_a} = \frac{\sigma}{R_0} - \omega. \quad (9)$$

The energy (6) can be expanded in a series in ϕ . Inserting Eq. (9) into Eq. (6), one sees that the term linear in ϕ vanishes. Ignoring higher order terms in $\partial_z \phi$, one gets $\Omega_a = \Omega_a(R_0) + \mathcal{H}[\phi]$, where $\Omega_a(R_0)$ is the energy of an unperturbed cylinder and

$$\mathcal{H}[\phi] = \int_0^L dz \left[\frac{\kappa}{2} (\partial_z \phi)^2 + V(\phi) \right]. \quad (10)$$

Here $\kappa = 2\pi\sigma R_0$ and

$$V(\phi) \equiv V_{shell}(R_0 + \phi) - V_{shell}(R_0) - \frac{\pi\sigma}{R_0} \phi^2. \quad (11)$$

Several minima in the potential $V(\phi)$, such as those corresponding to stable wires with conductance $G/G_0 = 3, 6, 17, 23, 42, 51, 96, \dots$ (cf. Fig. 1) can be locally approximated either by a bistable symmetric quartic potential

$$V^s(\phi) = \frac{1}{2}\eta\phi^2 - \frac{1}{4}\lambda\phi^4, \quad (12)$$

or by an asymmetric cubic potential

$$V^a(\phi) = -\alpha\tilde{\phi} + \frac{1}{3}\beta\tilde{\phi}^3, \quad (13)$$

where $\tilde{\phi} = \phi + \sqrt{\alpha/\beta}$. The latter potential biases fluctuations towards smaller radii ($\phi < 0$); however biases in the opposite direction are trivially accommodated by reflecting the potential so that $\tilde{\phi} \mapsto -\tilde{\phi}$ and redefining $\tilde{\phi} = \phi - \sqrt{\alpha/\beta}$.

The boundary conditions on ϕ are determined by the physics of the problem: Simulations of nanowire surface dynamics⁶ indicate that the cylindrical segment of a nanowire joins abruptly to a contact having the form of an unduloid of revolution (for which the electron-shell correction to the energy is suppressed by a finite slope), consistent with Neumann boundary conditions. This choice of boundary conditions is also consistent with the experimental finding¹ that thinning of a suspended nanowire occurs via nucleation of a surface kink at one end, as discussed in Sec. 5.

Finally, we note that in this paper, we consider a thermodynamic ensemble of nanowires at *fixed length* L . This implies that the ends of the wire are held fixed by a tensile force $F_{eq} = -\partial\Omega_e/\partial L$, which was calculated previously.^{4, 29, 32} Under elongation or compression at a finite rate, $F \neq F_{eq}$, and hence a different thermodynamic ensemble must be used. The dependence of nanowire lifetime on the applied force will be discussed elsewhere.³³

Eqs. (10-13) provide the starting point for our field-theoretic formulation of nanowire lifetimes, to be developed in the following sections.

4. ESCAPE PHENOMENOLOGY

The preceding discussion suggests that the problem of stability of nanowires against thermal fluctuations can be studied as a one-dimensional Ginzburg–Landau scalar field theory, perturbed by weak spatiotemporal noise, in a domain of finite extent. Problems of this type have recently received increasing attention. The classical nucleation problem on an *infinite* line was treated by Langer,³⁴ and its quantum analogue by Callan and Coleman,³⁵ in two influential and much-cited papers. However, the corresponding problem in a *finite* domain has been less intensively studied.^{36–38}

The difference between finite and infinite systems is not merely quantitative. For example, it was recently found that an unusual effect, analogous to a phase transition, occurs in an overdamped classical Ginzburg–Landau field theory with a bistable ϕ^4 potential. The transition occurs when the length L of its one-dimensional spatial domain is varied.^{39,40} Below a critical length L_c , the transition state is a spatially constant field configuration. However, at $L = L_c$ it bifurcates in the symmetric case into a spatially varying pair of configurations, degenerate in energy. The asymmetric potential of Eq. (13) shows a similar transition,⁴¹ but due to the asymmetry there is only a single preferred activation state. These studies demonstrate that the “phase transition” at a critical length L_c is reasonably robust.

As one would expect, the transition rate is strongly affected by the transition. Formally, the prefactor in the Kramers (weak-noise) nucleation rate *diverges* at $L = L_c$. This signals that precisely at $L = L_c$, escape from a stable state becomes *non-Arrhenius*: the rate at which it occurs falls off in the limit of weak noise not like an exponential (with a constant prefactor), but rather like an exponential with a power-law prefactor. An interesting consequence is that this transition may be observable in nanowire decay phenomenology.

The model as introduced in Sec. 3 treats ϕ , the fluctuations of the nanowire radius, as a classical field on a one-dimensional spatial domain $[0, L]$. Its dynamics are governed by the stochastic Ginzburg–Landau equation

$$\dot{\phi} = \kappa\phi'' - V'(\phi) + (2T)^{1/2}\xi(z, t), \quad (14)$$

where $\xi(z, t)$ is unit-strength spatiotemporal white noise, satisfying $\langle \xi(z_1, t_1)\xi(z_2, t_2) \rangle = \delta(z_1 - z_2)\delta(t_1 - t_2)$. In Eq. (14), time is measured in units of a microscopic timescale describing the short-wavelength cutoff of the surface dynamics,⁴ which is given to within a factor of order unity by the inverse Debye frequency ν_D^{-1} . The zero-noise dynamics is “gradient,” i.e., conservative. That is, at zero temperature

$$\dot{\phi} = -\delta\mathcal{H}/\delta\phi, \quad (15)$$

where $\mathcal{H}[\phi]$ is the energy functional, given by Eq. (10). So the statistical properties of the stochastically evolving field ϕ are described by equilibrium statistical mechanics. At nonzero temperature, however, thermal fluctuations can induce transitions between stable states (i.e., local minima) of the potential $V(\phi)$, which correspond in our model to different stable cylindrical radii, as discussed in Sec. 3. Such transitions occur via nucleation of a “droplet” of one stable configuration in the background of the other, subsequently quickly spreading to fill the entire spatial domain. When the noise is weak, i.e., at low temperatures (compared to the barrier height) most fluctuations will not succeed in nucleating a new phase; it is far more likely for a small droplet to shrink and vanish.

In the infinite-dimensional configuration space, a transition state must go “uphill” in energy from each stable field configuration. Because of exponential suppression of fluctuations as their energy increases, there is at low temperature a preferred transition configuration (saddle) that lies between adjacent minima. These are the nucleation pathways, in effect “paths of least resistance.” By time-reversal invariance, they are time-reversed zero-noise “downhill” trajectories.⁴² At low temperatures, the expected waiting time of the order parameter ϕ in a basin of attraction is an exponential random variable, as is typical of slow rate processes. The activation rate (the reciprocal of the mean time between flips) will be given in the $T \rightarrow 0$ limit by the Kramers formula

$$\Gamma \sim \Gamma_0 \exp(-\Delta E/T). \quad (16)$$

Here ΔE is the activation barrier, which quantifies the extent to which the preferred transition configuration between the two stable configurations is energetically disfavored; that is, ΔE is the energy of the transition state minus the energy of either stable state. Γ_0 is the rate prefactor.

The quantities ΔE and Γ_0 depend on the parameters of the potential, on the length L , and on the choice of boundary conditions at the endpoints $z = 0$ and $z = L$. The boundary conditions affect the way in which order parameter reversal occurs, since they may force nucleation to begin, preferentially, at the endpoints.

5. THE STABLE AND TRANSITION STATES

It will simplify the discussion to express the potentials in Eqs. (12) and (13) in dimensionless units.

For the symmetric potential Eq. (12), we can scale out the various constants by introducing the variables $x = \sqrt{\eta/\kappa}z$, $u = \sqrt{\lambda/\eta}\phi$, and $E_0 = \kappa^{1/2}\eta^{3/2}/\lambda$. The energy functional then becomes

$$\mathcal{H}[u]/E_0 = \int_0^{\ell^s} \left[\frac{1}{2}(u')^2 + \frac{1}{2}u^2 - \frac{1}{4}u^4 \right] dx \quad (17)$$

where $\ell^s = \sqrt{\eta/\kappa}L$.

For the asymmetric potential Eq. (13), we can scale out the various constants by introducing the variables $x = [(\alpha\beta)^{1/4}/\kappa^{1/2}]z$, $u = \sqrt{\beta/\alpha}\tilde{\phi}$, and $E_0 = \kappa^{1/2}\alpha^{5/4}/\beta^{3/4}$. The energy functional then becomes

$$\mathcal{H}[u]/E_0 = \int_0^{\ell^a} \left[\frac{1}{2}(u')^2 - u + \frac{1}{3}u^3 \right] dx \quad (18)$$

where $\ell^a = [(\alpha\beta)^{1/4}/\kappa^{1/2}]L$. These reduced potentials are shown in Fig. 2.

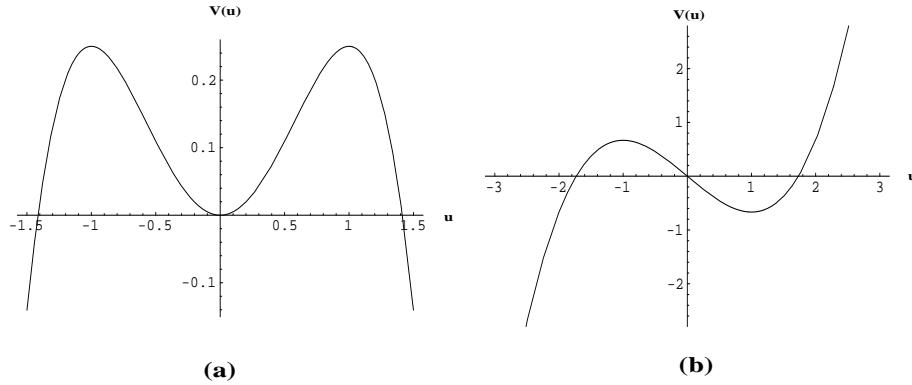


Figure 2. Potentials for the reduced order parameter u . (a) Symmetric case corresponding to Eq. (12). (b) Asymmetric case corresponding to Eq. (13).

In the absence of external noise, and with Neumann boundary conditions $u'(0) = u'(L) = 0$, the noiseless ($T = 0$) evolution equation (14) with either potential possesses both uniform and nonuniform stationary states. We turn now to their study.

5.1. Symmetric Potential

There are three constant time-independent solutions: $u = 0$, with energy 0, and $u = \pm 1$, with energy $1/4$. It is easy to see from Fig. 2 that $\phi = 0$ is stable for any L , and $\phi = \pm 1$ are always unstable; this is confirmed by eigenvalue analysis⁴¹ (see below).

What *nonconstant* time-independent solutions exist when $T = 0$? By Eqs. (10) and (15), any stationary solution satisfies $\dot{\phi} = -\delta\mathcal{H}/\delta\phi = 0$, yielding in this case the nonlinear ordinary differential equation

$$u'' = u - u^3. \quad (19)$$

The linearized noiseless dynamics in the vicinity of such a state are specified by the Hessian operator $\delta^2\mathcal{H}/\delta u^2$. Stability of stationary solutions is determined by eigenvalues of this operator. Those with all positive eigenvalues are stable; those with a single negative eigenvalue are potential transition states. (In the limit of low thermal noise, the actual transition state is that with the smallest energy difference with the relevant stable state.) The eigenvector corresponding to the negative eigenvalue is the direction (in the infinite-dimensional configuration space) along which the optimal escape trajectory approaches the saddle, in the limit of low noise.

Kink-like field configurations that asymptotically connect ground or vacuum states are often called *instanton states*, in a nomenclature derived from Callan and Coleman.³⁵ We will use the term “instanton” here for similar nonconstant solutions on finite domains.

When ℓ^s is finite, the instanton state(s) can be expressed in terms of *Jacobi elliptic functions*.⁴³ Such functions are characterized by an index m , $0 \leq m \leq 1$, which we shall see is related to ℓ^s through the boundary conditions. The instanton solution of Eq. (19) is the same as that for periodic boundary conditions,³⁸ but the dependence of ℓ^s on m differs:

$$u_{\text{inst},m}(x) = \pm \sqrt{\frac{2}{2-m}} \operatorname{dn}(x/\sqrt{2-m} \mid m), \quad (20)$$

where $\operatorname{dn}(\cdot \mid m)$ is the Jacobi elliptic dn function with parameter m . Its half-period is given by $\mathbf{K}(m)$, the complete elliptic integral of the first kind,⁴³ which is a monotonically increasing function of m . From a physical perspective such a solution, extended over the whole line, can be viewed as an infinite alternating sequence of kinks and anti-kinks, spaced a distance $\mathbf{K}(m)$ apart. As $m \rightarrow 0^+$, $\mathbf{K}(m)$ decreases to $\pi/2$, and $\operatorname{dn}(\cdot \mid m)$ degenerates to 1. As $m \rightarrow 1^-$, the half-period $\operatorname{dn}(\cdot \mid m)$ increases to infinity (with a logarithmic divergence), and $\operatorname{dn}(\cdot \mid m)$ degenerates to the nonperiodic function $\operatorname{sech}(\cdot)$, which is the canonical double-kink soliton. This limiting form is in fact the shape of the critical droplet pair in the Langer and Callan–Coleman analyses. (A good pedagogical discussion is given by Schulman⁴⁴).

It is easily seen that the solution Eq. (20) with lowest energy (i.e., fewest kinks) that satisfies the Neumann boundary condition requires

$$\ell^s = \sqrt{2-m}\mathbf{K}(m), \quad (21)$$

which in turn leads to $\ell_c^s = \pi/\sqrt{2}$. As $\ell^s \rightarrow \ell_c^s$ from above (i.e., $m \rightarrow 0^+$), $\operatorname{dn}(x|0) = 1$, and the instanton states reduce to the uniform unstable states $u_u = \pm 1$. This point corresponds to the *critical length* ℓ_c^s .^{39,40} If $\ell^s \leq \ell_c^s$

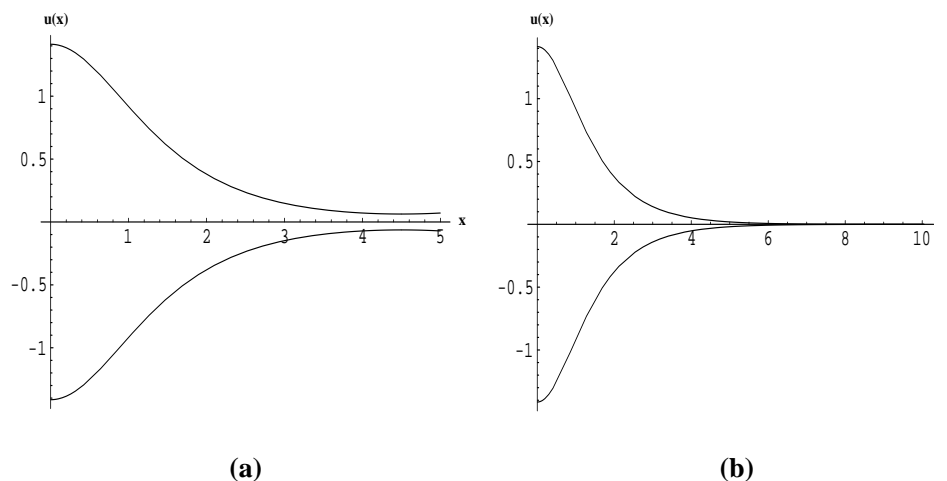


Figure 3. The two lowest-energy nonconstant transition states for the symmetric potential with Neumann boundary conditions, when (a) $\ell^s = 5$ and (b) $\ell^s = 10$. Because of the symmetry, each nonzero state has a degenerate counterpart obtained by $u \mapsto -u$. The width of the nonconstant portion of the instanton remains essentially constant for larger ℓ^s . The stable state for any ℓ^s is $u = 0$.

the transition state is one of the two uniform configurations $u = \pm 1$. As $m \rightarrow 1^-$, $\ell \rightarrow \infty$, and the instanton state becomes

$$u_{\text{inst},1}(x) = \sqrt{2}\text{sech}(x) \quad (22)$$

The nonconstant transition states for the symmetric potential case with Neumann boundary conditions are plotted in Fig. 3. Of course, by the symmetry in the problem the instanton can nucleate with equal probability at either end; this is manifested by the existence of degenerate solutions (not shown) in which x is replaced by $L - x$ in Eq. (20). This will be true for the asymmetric case as well, and the existence of solutions reflected about the midpoint of the interval will be tacitly understood from now on.

5.2. Asymmetric Potential

Here the time-independent solutions of the zero-noise Ginzburg-Landau equation (i.e., extremal states of $\mathcal{H}[\phi]$) satisfy

$$u'' = -1 + u^2. \quad (23)$$

With Neumann boundary conditions, there is a uniform stable state $u_s = +1$, and a uniform unstable state $u_u = -1$. The latter is the transition state for $\ell^a < \ell_c^a = \pi/\sqrt{2}$. At ℓ_c^a a transition occurs, and above it the transition state is nonuniform.

In the asymmetric case the instanton solution is⁴¹

$$u_{\text{inst},m}(x) = \frac{2-m}{\sqrt{m^2-m+1}} - \frac{3}{\sqrt{m^2-m+1}} \text{dn}^2\left(\frac{x}{\sqrt{2}(m^2-m+1)^{1/4}} \middle| m\right). \quad (24)$$

It is easily seen that this solution satisfies the Neumann boundary condition with lowest energy when

$$\ell^a = \sqrt{2}(m^2 - m + 1)^{1/4} \mathbf{K}(m), \quad (25)$$

which in turn leads to $\ell_c^a = \pi/\sqrt{2}$, as noted above. (The fact that the critical lengths in the symmetric and asymmetric case are equal is coincidental.) As $\ell^a \rightarrow \ell_c^a$ from above (i.e., $m \rightarrow 0^+$), $\text{dn}(x|0) = 1$, and the instanton state reduces to the uniform unstable state $u_u = -1$. As $m \rightarrow 1^-$, $\ell \rightarrow \infty$, and the instanton state becomes

$$u_{\text{inst},1}(x) = 1 - 3\text{sech}^2\left(\frac{x}{\sqrt{2}}\right) \quad (26)$$

The stable and transition states for the asymmetric potential case with Neumann boundary conditions are shown in Fig. 4.

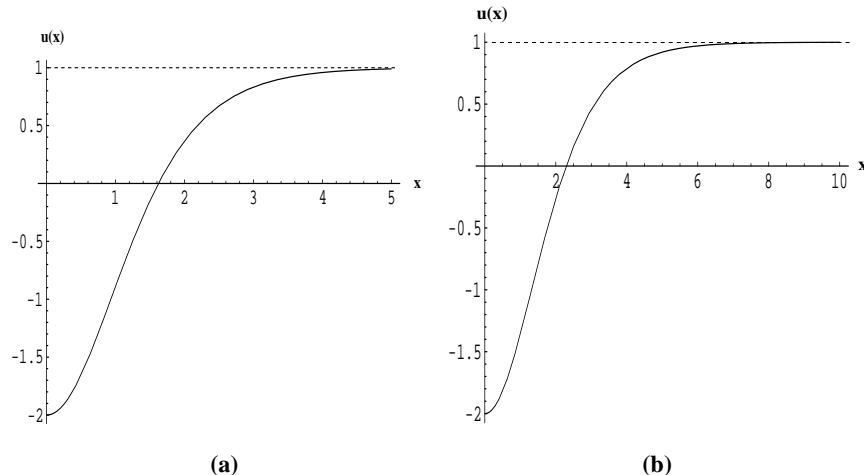


Figure 4. The stable state (dashed line) and nonconstant transition state (solid line), for the asymmetric potential with Neumann boundary conditions, when (a) $\ell^a = 5$ and (b) $\ell^a = 10$. The width of the nonconstant portion of the instanton remains essentially constant for larger ℓ^a .

6. THE ACTIVATION BARRIER

As mentioned in Sec. 4, the exponential falloff of the transition rate in the limit of weak thermal noise, i.e., its Arrhenius behavior, is determined by the activation barrier (sometimes called the “activation energy”) ΔE between the stable and instanton states. ΔE is defined to be $(\mathcal{H}[\phi_u] - \mathcal{H}[\phi_s])$, with the energy functional $\mathcal{H}[\phi]$ given by Eq. (10). The calculation of $\mathcal{H}[\phi_s]$ and $\mathcal{H}[\phi_u]$, the stable and transition state energies, is trivial in the case of uniform states. It remains reasonably straightforward in the case of the instanton states for the models studied here, and can be expressed in terms of complete elliptic integrals.⁴³ The results are as follows:

Symmetric potential.—If $\ell^s \leq \ell_c^s = \pi/\sqrt{2}$, then the transition state is one of the two uniform configurations $u = \pm 1$, and $\Delta E/E_0 = \ell^s/4$. If $\ell^s > \ell_c^s$, then

$$\Delta E^s/E_0 = \frac{1}{3\sqrt{2-m}} \left[2\mathbf{E}(m) - \frac{1-m}{2-m}\mathbf{K}(m) \right]. \quad (27)$$

The activation energy in the $\ell^s \rightarrow \infty$ limit equals $2/3$, which is the energy of a single kink.

The above formula for the activation energy ΔE^s as a function of ℓ^s is plotted in Fig. 5. The transition at $\ell_c^s = \pi/\sqrt{2}$ is apparent, as is the differentiability (and lack of twice differentiability) through the transition.

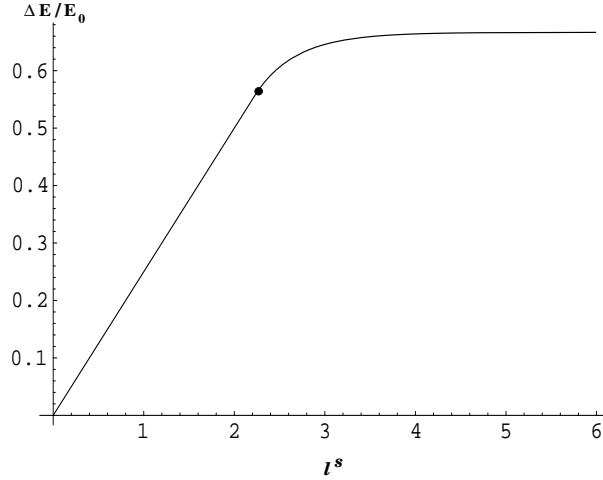


Figure 5. The activation energy ΔE^s as a function of the interval length ℓ , for the symmetric potential with Neumann boundary conditions. The bullet indicates the critical interval length $\ell_c^s = \pi/\sqrt{2}$ at which the transition takes place.

Asymmetric potential.—If $\ell^a \leq \ell_c^a = \pi/\sqrt{2}$, then the transition state is the uniform configuration $u = -1$, and $\Delta E^a/E_0 = (4/3)\ell^a$. If $\ell^a > \ell_c^a$, then

$$\frac{\Delta E^a}{E_0} = \left[\frac{2-3m-3m^2+2m^3}{3(m^2-m+1)^{3/2}} + \frac{2}{3} \right] \ell^a + \frac{6\sqrt{2}}{5(m^2-m+1)^{1/4}} \left[2\mathbf{E}(m) - \frac{(2-m)(1-m)}{(m^2-m+1)}\mathbf{K}(m) \right]. \quad (28)$$

There is a difference of a factor of 2 in the second term of the RHS with respect to the corresponding formula in Ref.⁴¹; this results from the different boundary condition employed in that paper. As $\ell \rightarrow \infty$, $\Delta E^a/E_0 \rightarrow 12\sqrt{2}/5$. The activation barrier for the entire range of ℓ is shown in Fig. 6.

7. THE TRANSITION RATE PREFACTOR

Calculation of the prefactor Γ_0 in the Kramers transition rate formula (16) is a much more involved matter than the computation of ΔE . It generally requires an analysis of the *transverse fluctuations* about the instanton solutions. The general method applied to the present set of problems has been discussed elsewhere.^{39–41} In

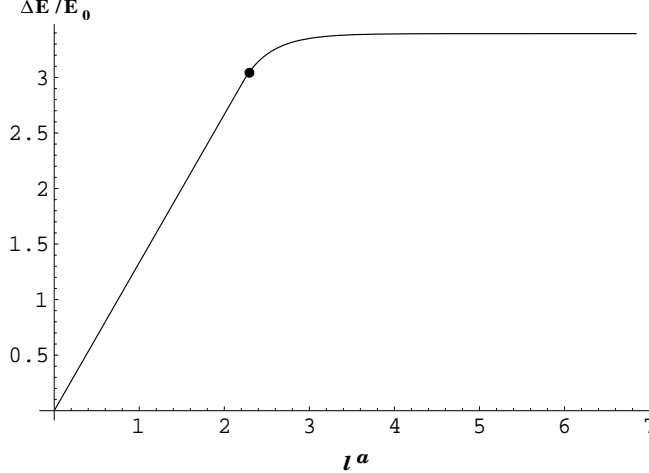


Figure 6. The activation energy ΔE^a as a function of the interval length ℓ^a , for the asymmetric potential with Neumann boundary conditions. The bullet indicates the critical interval length $\ell_c^a = \pi/\sqrt{2}$ at which the transition takes place.

the present article, we focus on the most technologically relevant regime $L \gg L_c$, in which the prefactor is $O(1)$ in natural units, i.e., $\Gamma_0 \approx \nu_D$. We defer discussion of the prefactor in shorter wires with $L \lesssim L_c$ to a later publication.³³

8. DISCUSSION

Pulling together the results from the preceding sections, our continuum dynamical model predicts that the lifetime τ of a metastable cylindrical nanowire of length greater than the critical length L_c is given by

$$\frac{1}{\tau} = \Gamma \approx \nu_D \exp(-\Delta E_\infty/T), \quad (29)$$

where ν_D is the Debye frequency and $\Delta E_\infty = \lim_{L \rightarrow \infty} \Delta E$ is the activation barrier for a long wire. Note that for a moderately thick wire with $G/G_0 \gg 1$, the lifetime τ may not be the typical time before the wire breaks, but rather a switching time between two different metastable wires with different conductance values. In terms of the physical parameters defined in section 3, $\Delta E_\infty = \frac{2}{3}\kappa^{1/2}\eta^{3/2}/\lambda$ for the case of a symmetric quartic potential well (12) and $\Delta E_\infty = \frac{12\sqrt{2}}{5}\kappa^{1/2}\alpha^{5/4}/\beta^{3/4}$ for the case of an asymmetric cubic potential well (13). The lifetimes for several cylindrical sodium and gold nanowires, calculated using the best cubic- or symmetric quartic-polynomial fits to the potential (11), are tabulated in Table 1.

An important prediction given in Table 1 is that the lifetimes of the most stable nanowires, while they do exhibit significant variations from one conductance plateau to another, do not vary systematically as a function of radius; the activation barriers in Table 1 vary by only about 30% from one plateau to another, and the wire with a conductance of $96G_0$ has essentially the same lifetime as that with a conductance of $3G_0$. In this sense, the activation barrier appears to exhibit *universal mesoscopic fluctuations*: in any conductance interval, there are very short-lived wires (not shown in Table 1) with very small activation barriers, while the longest-lived wires have activation barriers of a universal size:

$$0 < \Delta E_\infty \lesssim 0.7 \left(\frac{\hbar^2 \sigma}{m_e} \right)^{1/2}, \quad (30)$$

where σ is the surface tension and m_e is the free-electron rest mass. The scaling with σ in Eq. (30) follows straightforwardly if one neglects the third term on the right hand side of Eq. (11), which is a small correction that tends to destabilize the wires, and is more important in gold than in sodium.

Table 1. The lifetime τ (in seconds) for various cylindrical sodium and gold nanowires at temperatures from 75K to 200K. Here G is the electrical conductance of the wire, L_c is the critical length above which the lifetime may be approximated by $\tau \approx \nu_D^{-1} \exp(\Delta E_\infty/T)$, ΔE_∞ is the activation energy for an infinitely long wire, and ν_D is the Debye frequency. Note that wires shorter than L_c are predicted to have shorter lifetimes.

G [G_0]	Na					Au				
	L_c [nm]	ΔE_∞ [meV]	τ [s]			L_c [nm]	ΔE_∞ [meV]	τ [s]		
			75 K	100 K	150 K			100 K	150 K	200 K
3	1.4	210	30	9×10^{-3}	3×10^{-6}	1.5	470	10^{11}	2×10^3	0.2
6	2.6	170	0.06	9×10^{-5}	10^{-7}	3.0	310	10^3	7×10^{-3}	2×10^{-5}
17	3.1	230	500	0.08	10^{-5}	3.4	470	9×10^{10}	10^3	0.2
23	3.7	190	4	2×10^{-3}	10^{-6}	4.1	390	10^7	3	2×10^{-3}
42	4.3	210	50	0.01	4×10^{-6}	4.8	440	3×10^9	100	0.03
51	4.5	150	7×10^{-3}	2×10^{-5}	5×10^{-8}	4.9	320	2×10^3	0.01	3×10^{-5}
96	5.8	200	5	2×10^{-3}	10^{-6}	6.3	440	8×10^9	300	0.05

The lifetimes tabulated for sodium nanowires in Table 1 exhibit a rapid decrease in the temperature interval between 75K and 100K. This behavior can explain the observed temperature dependence of conductance histograms for sodium nanowires,^{20–22} which show clear peaks at conductances near the predicted values at temperatures up to 100K, but were not reported at higher temperatures. A comparison of the lifetimes of sodium and gold nanowires listed in Table 1 indicates that gold nanowires are much more stable, as expected from the larger value of the surface tension $\sigma_{\text{Au}} = 5.9 \sigma_{\text{Na}}$. This is consistent with the observation that gold nanowires in particular, and noble metal nanowires in general, are much more stable than alkali metal nanowires. However, the calculated lifetimes of gold nanowires are not sufficient to account for the observed stability of gold nanowires at room temperature and above. This quantitative discrepancy may arise due to the neglect of d-electrons in our model (except in as much as they enhance σ compared to the free-electron value), which are believed to play an important role in gold nanostructures.

ACKNOWLEDGMENTS

J.B. and C.A.S. acknowledge support from NSF Grant No. DMR0312028. D.L.S. acknowledges support from NSF Grant Nos. PHY0099484 and PHY0351964.

REFERENCES

1. Y. Kondo and K. Takayanagi, “Gold nanobridge stabilized by surface structure,” *Phys. Rev. Lett.* **79**, pp. 3455–3458, 1997.
2. Y. Kondo and K. Takayanagi, “Synthesis and characterization of helical multi-shell gold nanowires,” *Science* **289**, pp. 606–608, 2000.
3. F. Kassubek, C. A. Stafford, H. Grabert, and R. E. Goldstein, “Quantum suppression of the Rayleigh instability in nanowires,” *Nonlinearity* **14**, pp. 167–177, 2001.
4. C.-H. Zhang, F. Kassubek, and C. A. Stafford, “Surface fluctuations and the stability of metal nanowires,” *Phys. Rev. B* **68**, p. 165414, 2003.
5. D. F. Urban and H. Grabert, “Interplay of Rayleigh and Peierls instabilities in metallic nanowires,” *Phys. Rev. Lett.* **91**, p. 256803, 2003.
6. J. Bürki, R. E. Goldstein, and C. A. Stafford, “Quantum necking in stressed metallic nanowires,” *Phys. Rev. Lett.* **91**, p. 254501, 2003.
7. N. Agrait, J. G. Rodrigo, and S. Vieira, “Conductance steps and quantization in atomic-size contacts,” *Phys. Rev. B* **47**, pp. 12345–12348, 1993.

8. G. Rubio, N. Agraït, and S. Vieira, "Atomic-sized metallic contacts: mechanical properties and electronic transport," *Phys. Rev. Lett.* **76**, pp. 2302–2305, 1996.
9. A. Stalder and U. Dürig, "Study of yielding mechanics in nanometer-sized Au contacts," *Appl. Phys. Lett.* **68**, pp. 637–639, 1996.
10. M. Brandbyge, J. Schiøtz, M. R. Sørensen, P. Stoltze, K. W. Jacobsen, J. K. Nørskov, L. Olesen, E. Lægsgaard, I. Stensgaard, and F. Besenbacher, "Quantized conductance in atom-sized wires between two metals," *Phys. Rev. B* **52**, pp. 8499–8514, 1995.
11. J. M. Krans, J. M. van Ruitenbeek, V. V. Fisun, I. K. Yanson, and L. J. de Jongh, "The signature of conductance quantization in metallic point contacts," *Nature* **375**, pp. 767–769, 1995.
12. J. L. Costa-Krämer, N. García, P. García-Mochales, P. A. Serena, M. I. Marqués, and A. Correia, "Conductance quantization in nanowires formed between micro and macroscopic metallic electrodes," *Phys. Rev. B* **55**, pp. 5416–5424, 1997.
13. A. I. Yanson, G. Rubio Bollinger, H. E. van den Brom, N. Agraït, and J. M. van Ruitenbeek, "Formation and manipulation of a metallic wire of single gold atoms," *Nature* **395**, pp. 783–785, 1998.
14. N. Agraït, A. Levy Yeyati, and J. M. van Ruitenbeek, "Quantum properties of atomic-sized conductors," *Phys. Rep.* **377**, pp. 81–279, 2003.
15. C. J. Muller, J. M. van Ruitenbeek, and L. J. de Jongh, "Experimental observation of the transition from weak link to tunnel junction," *Phys. C* **191**, pp. 485–504, 1992.
16. D. F. Urban, J. Bürki, A. I. Yanson, I. K. Yanson, C. A. Stafford, J. M. van Ruitenbeek, and H. Grabert, "Electronic shell effects and the stability of alkali nanowires." submitted to Solid State Communications, 2004.
17. P. García-Mochales and P. A. Serena, "Disorder as origin of residual resistance in nanowires," *Phys. Rev. Lett.* **79**, pp. 2316–2319, 1997.
18. J. Bürki, C. A. Stafford, X. Zotos, and D. Baeriswyl, "Cohesion and conductance of disordered metallic point contacts," *Phys. Rev. B* **60**, pp. 5000–5008, 1999.
19. J. Bürki and C. A. Stafford, *Statistics of quantum transport in metal nanowires with surface disorder*, pp. 27–30. in *Electronic Correlations: from meso- to nano-physics*, edited by T. Martin, G. Montambaux, and J. Trần Thanh Vân, EDP Sciences, Les Ulis, France, 2001.
20. A. I. Yanson, I. K. Yanson, and J. M. van Ruitenbeek, "Observation of shell structure in sodium nanowires," *Nature* **400**, pp. 144–146, 1999.
21. A. I. Yanson, I. K. Yanson, and J. M. van Ruitenbeek, "Supershell structure in alkali metal nanowires," *Phys. Rev. Lett.* **84**, pp. 5832–5835, 2000.
22. A. I. Yanson, J. M. van Ruitenbeek, and I. K. Yanson, "Shell effects in alkali metal nanowires," *Low Temp. Phys.* **27**, pp. 807–820, 2001.
23. M. Díaz, J. L. Costa-Krämer, E. Medina, A. Hasmy, and P. A. Serena, "Evidence of shell structures in Au nanowires at room temperature," *Nanotech.* **14**, pp. 113–116, 2003.
24. A. I. Mares, A. F. Otte, R. H. M. Smit, and J. M. van Ruitenbeek, "Observation of electronic and atomic shell effects in gold nanowires." Preprint, cond-mat/0401330, 2004.
25. H. Ohnishi, Y. Kondo, and K. Takayanagi, "Quantized conductance through individual rows of suspended gold atoms," *Nature* **395**, pp. 780–783, 1998.
26. M. Okamoto and K. Takayanagi, "Structure and conductance of a gold atomic chain," *Phys. Rev. B* **60**, pp. 7808–7811, 1999.
27. V. Rodrigues, T. Fuhrer, and D. Ugarte, "Signature of atomic structure in the quantum conductance of gold nanowires," *Phys. Rev. Lett.* **85**, pp. 4124–4127, 2000.
28. Y. Oshima, A. Onga, and K. Takayanagi, "Helical gold nanotube synthesized at 150 K," *Phys. Rev. Lett.* **91**, p. 205503, 2003.
29. C. A. Stafford, D. Baeriswyl, and J. Bürki, "Jellium model of metallic nanocoherence," *Phys. Rev. Lett.* **79**, pp. 2863–2866, 1997.
30. D. F. Urban, J. Bürki, C.-H. Zhang, C. A. Stafford, and H. Grabert, "Jahn-Teller distortions and the supershell effect in metal nanowires." cond-mat/0312517, 2003.

31. M. Brack and R. K. Bhaduri, *Semiclassical physics*, vol. 96 of *Frontiers in physics*, Edited by David Pines, Addison-Wesley publishing company, Inc., 1997.
32. C. A. Stafford, F. Kassubek, J. Bürki, and H. Grabert, “Universality in metallic nanocoherence: A quantum chaos approach,” *Phys. Rev. Lett.* **83**, pp. 4836–4839, 1999.
33. J. Bürki, C. A. Stafford, and D. L. Stein. unpublished, 2004.
34. J. S. Langer, “Statistical theory of the decay of metastable states,” *Ann. Phys.* **54**, pp. 258–275, 1969.
35. C. G. Callan and S. Coleman, “Fate of the false vacuum, ii: First quantum corrections,” *Phys. Rev. D* **16**, pp. 1762–1768, 1977.
36. W. G. Faris and G. Jona-Lasinio, “Large fluctuations for a nonlinear heat equation with noise,” *J. Phys. A* **15**, pp. 3025–3055, 1982.
37. F. Martinelli, E. Oliveira, and E. Scoppola, “Small random perturbations of finite and infinite dimensional dynamical systems: Unpredictability of exit times,” *J. Stat. Phys.* **55**, pp. 477–504, 1989.
38. A. J. McKane and M. B. Tarlie, “Regularization of functional determinants using boundary perturbations,” *Phys. Rev. E* **28**, pp. 6931–6942, 1995.
39. R. S. Maier and D. L. Stein, “Droplet nucleation and domain wall motion in a bounded interval,” *Phys. Rev. Lett.* **87**, p. 270601, 2001.
40. R. S. Maier and D. L. Stein, “Effects of weak spatiotemporal noise on a bistable one-dimensional system,” in *Noise in Complex Systems and Stochastic Dynamics*, L. Schimansky-Geier, D. Abbott, A. Neiman, and C. V. den Broeck, eds., pp. 67–78, SPIE, Singapore, 2003.
41. D. L. Stein, “Critical behavior of the Kramers escape rate in asymmetric classical field theories,” *J. Stat. Phys.* **114**, pp. 1537–1556, 2004. Available as cond-mat/0311263.
42. R. S. Maier and D. L. Stein, “The escape problem for irreversible systems,” *Phys. Rev. E* **48**, pp. 931–938, Aug 1993.
43. M. Abramowitz and I. A. Stegun, eds., *Handbook of Mathematical Functions*, Dover, New York, 1965.
44. L. S. Schulman, *Techniques and Applications of Path Integration*, Wiley, New York, 1981.